CLM-R 227

CLM-R 227

UKAEA

Report

SOFT X-RAY IMAGING DIAGNOSTIC ON THE HBTX 1A REVERSED FIELD PINCH

M. MALACARNE
I. H. HUTCHINSON

CULHAM LABORATORY
Abingdon Oxfordshire

1982

C/18

Available from H. M. Stationery Office

£2.00

CLM-R 227

SOFT X-RAY IMAGING DIAGNOSTIC ON THE HBTX 1A REVERSED FIELD PINCH

M Malacarne*, I H Hutchinson

Culham Laboratory, Abingdon, Oxon, OX14 3DB, U.K.

(EURATOM-UKAEA Fusion Association)

Abstract

A pinhole camera with an array of surface barrier diodes has been used with appropriate filters to detect soft X-ray emission from the central region of the HBTX IA reversed field pinch plasma.

Here we discuss the application in which the internal fluctuations of the plasma are measured. These include a significant turbulent component as well as more coherent modes. For this reason spectral and correlation analysis techniques are more appropriate than the usual tomographic approach. These indicate the different correlation lengths for different fluctuation frequencies.

(* Euratom supported fellow)

September 1982

ISBN 0 85311 111 1

1. INTRODUCTION

The method of imaging of soft X-ray emission onto multiple detectors has become widely used on tokamak plasmas (1-5). It has proven a particularly powerful technique for investigating large scale coherent perturbations arising from MHD instabilities (6). We describe here some of the details of the first systematic application of soft X-ray imaging to the diagnosis of a Reversed Field Pinch (RFP) plasma.

The reversed field pinch HBTX IA has the following parameters:

Major Radius	$R_o = 0.80$ m
Minor Radius	$a = 0.26$ m
Toroidal Current	$I_p \lesssim 500$ kA
Discharge Duration	$\lesssim 8$ ms
Typical Density	$n_e = 2 - 20 * 10^{19}$ m^{-3}
Typical Temperature	$T_e \lesssim 200$ eV

Thus in the parameters except for temperature and duration, the plasma is similar to tokamak plasmas. Another difference, apart from T_e, is that the general level of turbulence of the RFP is much greater than in the tokamak. As we shall see, these features lead to important differences in technique both of measurement and of analysis.

Because of the complicated dependence of X-ray emission intensity on density, temperature and impurity (7,8) it is very difficult to obtain absolute estimates of these parameters from the broad band measurements we are concerned with. Usually therefore, one concentrates

on the relative variation of the intensity in deducing the nature of various profiles and instabilities, relying on the fact that the intensity is a strong (exponential) function of temperature to ensure that temperature variation is the dominant effect. We adopt essentially this approach.

In section 2.1 the configuration of the imaging array is described. It is a fairly standard type of pinhole camera arrangement. The spectral response of detectors and filters is described in section 2.2. Because of the rather low electron temperature, non-standard filters are used to obtain the desired low-energy cut-off. The frequency response and noise performance of the system, which are determined largely by the preamplifier electronics, are described in 2.3. We then describe some typical results obtained from the diagnostic. Section 3.1 shows examples of the time evolution of the signal and its interpretation. The following two sections describe some analysis techniques which have been applied to the signals. These differ from the tomographic approach adopted in tokamaks because we find that the perturbations in the plasma are much more turbulent and incoherent. For this reason the statistical techniques of spectrum analysis (3.2) and of correlation analysis (3.3) are in many respects more appropriate. Finally we discuss the significance of the results so far and indicate some possible future directions for development and application of the techniques.

2. DESCRIPTION OF THE DIAGNOSTIC

2.1 Camera configuration

In its general outline this diagnostic consists of a series of X-ray detectors (aranged in one or more arrays) each viewing a different chord of the plasma column, in order to recreate a two dimensional picture of a minor cross section. The detector field of view is determined by its position relative to a front aperture - as in a pinhole camera - and by a variable size rear aperture placed just in front of the detector. These two apertures, their relative distance and the distance between the detectors determine the spatial resolution and the field of sight of the single array. Each detector is most sensitive to the densest and hottest region of plasma near the axis so that the distance between the chords in the proximity of the axis can be considered as a good approximation for their average separation. The whole diagnostic can consist of one or more of such arrays placed at different poloidal (and/or toroidal) positions.

In fig. 1 the geometry of apparatus is shown. In the present stage of development of the experiment only the central lower porthole is occupied by an array of eight surface barrier diodes. In future it is planned to include two more vertical arrays on the outer lower portholes and a horizontal one as well.

There are several detector types available for such a configuration but most usually surface barrier diodes (SBD) are chosen

for their high X-ray efficiency, good time resolution and ease of operation and calibration (for a comparison of this type of detector with others (see ref. 9). A filter has to be placed in front of each detector in order to shield it from unwanted visible light and to tailor its response to the characteristic features of the plasma.

2.2 Spectral response of detectors and filters

Whenever an absolute measurement of the intensity of the X-ray radiation from the plasma is required, it becomes necessary to carry out an accurate calibration of the photon efficiency of the detectors and of the transmissivity of the filters. The detectors we used were silicon surface barrier diodes (SBD) ORTEC BA-023-50-100. In this semiconductor device a rectifying junction is obtained by depositing a thin layer of gold (200 Å) on a wafer of n-doped silicon. Each photon that reaches the sensitive region inside the silicon (depletion region) produces an electron-hole pair per 3.6 eV of energy deposited (see ref. 9). The number of photons absorbed in the depletion layer (whose thickness is a function of the applied bias voltage and of the intrinsic resistivity of the material) depends on the transmissivity of the gold layer, of a silicon dead region at the junction and of the depletion layer, as well as on the transmissivity of the filters.

The original spectral distribution of emitted radiation (from the plasma) is therefore modified by the photon efficiency of the detecting system. Theoretical values of the attenuation coefficients in the range of energies we are concerned with (100 - 1000 eV, ultra-soft X-ray region) have been calculated or measured by many authors (ref. 10, 11, 12, 13). The surface barrier diodes have an intrinsic lower energy

cut-off at 3.6 eV. For plasma temperatures of 100 eV this means that we must concern ourselves also with the efficiency of the detectors in the VUV region where most of the emission will appear (ref. 14, 15, 16). It was discovered, for instance, that aluminium (which is commonly used for filters on tokamaks) is not suitable for our range of temperatures, owing to a window between 30 eV and 70 eV (see fig. 2) which is likely to contain most of the line radiation. We wish to exclude line radiation and concentrate on the continuum. It appears that silver does not present this problem and is thin in the region 100 - 400 eV. Figs. 2 and 3 show the transmissivity curve of a thin film (2000 Å) of aluminium and silver, respectively.

Another possible solution is offered by plastic films (polypropylene) coated with thin layers of metals. The transmissivity of polypropylene is shown in fig. 4. This material has good mechanical properties as opposed to thin metal foils which very often show presence of pinholes and are extremely fragile (they often break simply because of mechanical vibrations during the discharge). On the other hand, polypropylene has the disadvantage of being more opaque than silver in the region of 100 - 400 eV.

As for the efficiency of the detector, an estimated curve is shown in fig. 5. The absorption in the depletion region, for these energies, is complete so that the efficiency is governed by transmittance in the thin gold coating (200 Å) and in the dead region (for which we have assumed a thickness of 1500 Å). As can be seen, the efficiency in the interval 100 - 400 eV (the most important for us) is very poor, due to the presence of the dead silicon layer. The process whereby this dead

region is formed is still not very clear and no precise information on its thickness is available (ref. 17). If we want to exclude the VUV region (below 100 eV) but require the highest intensity, we must avoid any filter with a bad performance between 100 and 400 eV (such as aluminium). If we also require an absolute calibration of the detector, an experimental measurement of the thickness of the dead region is desirable.

The most convenient solution for the calibration of a SBD is to use a standard laboratory hot cathode X-ray source. In this arrangement a hot tungsten filament fluoresces characteristic lines from a metal target (made of materials such as Al, Be, C, S, Mg, etc.). Usually a flow proportional counter is used as a reference monitor. Ref. 18 describes the results of a calibration done with this method at the energies: 1487 eV (Al K_α) and 278 eV (C K_α).

A preliminary calibration was carried out on our detectors to check for differences in relative response (relevant to the study of radial profiles). The Al K_α line was used (the expected efficiency is very close to one) and a good agreement was found, within the experimental accuracy of about 10% , on a sample of five detectors. It is planned to repeat these measurements on a larger number of detectors and using lines at lower energies, e.g., the O K_α line, the C K_α line and eventually the Be K_α 109 eV line (just above the Si absorption edge). However, severe problems of X-ray intensity are expected to arise.

Linearity of detector response with photon intensity, independence from temperature and other similar results have been reported in ref. 18 .

2.3 Electronics, frequency response & noise

The surface barrier diode acts essentially as a current source in parallel with a capacitance of about 50 pF (at 15 V bias). Each diode is connected by a short coaxial cable (minimising the additional capacitance) to a current-to-voltage preamplifier which determines the frequency response and, in large measure, the noise performance. The circuit of each preamplifier is shown in fig. 6. The upper frequency response is determined by the feedback capacitors C_3, C_4. They give a theoretical 3dB bandwidth of about 200 kHz, which is suitable for our present application. This bandwidth has been confirmed by experimental calibration using a modulated LED source. Response is flat at lower frequencies and equal to 2.2 V/μA. The first stage is AC coupled with a very long time constant (47 s) which avoids offset and drift, except due to leakage currents in the coupling capacitors (C_1 and C_2). Thus the low frequency cut-off is 0.003 Hz which for our purposes is effectively DC. The preamplifier is capable of driving a 75Ω line, although only to 2 V.

The important noise sources arise due to thermal (Johnson) noise in the feedback resistor R_1 and the input noise of the first stage operational amplifier. With the LF357 integrated circuit as indicated the effective input noise level is about 1 $pA/Hz^{\frac{1}{2}}$ in the frequencies of interest. This can be improved somewhat at higher frequencies by using a NE5534A op-amp instead but our measurements have all been done with the LF357. The equivalent output noise is 2.2 $V/Hz^{\frac{1}{2}}$.

In many cases the dominant noise arises not from these thermal sources but from the photon statistics of X-ray arrival. We estimate

this effect as follows:

Suppose each photon on average gives rise to N electron-hole pairs and let the transimpedence of the amplifier be R (Volts/Amp). Then if the mean photon arrival rate is λ the mean output voltage is:

$$\bar{V} = eNR\lambda \quad (V)$$

The fluctuations in V due to photon statistics may readily be shown (19) to have a power spectrum P(f) - at frequency f - given by:

$$P(f) = 2\bar{V}^2/\lambda = 2eNR\bar{V} \quad (V^2/Hz).$$

Taking N = 100 (corresponding to typical photon energy 350 eV) and our value $R = 2.2*10^6$, we obtain:

$$P(f) = 7.0*10^{-11}\ \bar{V} \quad (V^2/Hz)$$

i.e., an output r.m.s. noise of $8.4*\bar{V}^{\frac{1}{2}}$ ($\mu V/Hz^{\frac{1}{2}}$). This is greater than the thermal noise if $\bar{V} > 70$ mV. So except for cases where the signal is very small, photon noise tends to be the more important source.

3 ANALYSIS OF THE DATA

3.1 Preliminary analysis

During the few months HBTX IA has been operative our main efforts were devoted to installing and testing the first of three planned SBD arrays. Different arrangements of filters were also tested. At the moment we adopt two solutions: a thin silver foil (2000 Å approx.) and a polypropylene film (1 μm) coated with silver (1000 Å) and aluminium (200 Å).

Some typical signals obtained with these two arrangements are shown in fig. 7 and 8, together with the plasma current (I_p) and the toroidal magnetic field at the wall (B_{Tw}), for a typical discharge at low current and at high current. SBD 3 is covered with a polypropylene filter while SBD 6 with a silver one. The peak value for electron density was $0.5*10^{14} cm^{-3}$ in both cases. The signal from the diodes starts some hundred microseconds after the current has risen: at the beginning of the discharge the input power goes into ionization and the electron temperature is still very low, most of the emission is in the VUV region (line radiation). This was confirmed by observations using aluminium filters in which case the output from the diodes started in coincidence with the plasma current.

From these plots one can immediately notice the absence of large amplitude coherent modes - such as those described for tokamak experiments (sawtooth oscillations etc.) - although some kind of

regular motions can be distinguished at times. In general however it was clear from the beginning that a study of instabilities of the type adopted on larger tokamak experiments has to be ruled out or at least substantially modified.

On the other hand, some evidence of global motion of the plasma has been found in a study of the off-axis displacement of the centroid of the signals (20) that contradicts our first impression of absence of coherent modes. Oscillations occur of the axis of symmetry of the emission around the geometrical axis of the vacuum chamber. It was also found that these oscillations are well correlated with similar data from magnetic coils.

3.2 Spectrum analysis

In order to gain a better understanding of the general picture, a preliminary spectrum analysis has been carried out. In parallel to this, a more precise correlation analysis was performed, which will be discussed in the next section.

It is well known that both spectrum and correlation analysis require ensemble averages to be made on several similar discharges in order to reduce the influence of random noise and to extract hidden periodicities from the bulk of fluctuations. This caused us not a little problem, owing to the scarcity of available data of good quality (saturation of the preamplifier or amplifier response alters completely the shape of the spectrum, for instance). In what follows, an ensemble average has always been made on 8-10 consecutive discharges.

The fundamental tool in our numerical manipulations is a Fast Fourier Transform algorithm that has been implemented on a PDP-11 computer system (for details of this program see ref. 21 , par. 2.1). The theory of Fourier analysis and its digital applications is widely known and used and will not be described here (see ref. 22 , 23, 24 , 25). A general consideration has to be made however about the usual assumption of stationarity and ergodicity of the process in question: in our case both conditions can be reasonably satisfied for time intervals not longer than 300 -500 μs (even less at the beginning of the discharge). The frequency resolution corresponding to such intervals (according to the sampling theorem) is about 2 -5 kHz. If low frequency modes of this same order of magnitude are investigated it becomes necessary to extend the computation to longer periods at the expense of accuracy. Therefore most of the following results will not pretend to be too rigorous. (The theory of nonstationary random processes is reported in ref. 25 , 26).

According to the energy of the fluctuations we distinguish roughly two different periods within the discharge: the setting-up phase, in which the current reaches its peak, the magnetic field reverses and large oscillations (especially at low frequencies) are visible, and the quiescence period, which starts after the plasma current has reached its peak value and where the whole spectrum decreases in energy and becomes flatter. Figs. 9 and 10 show the ensemble average power spectrum for the two phases in the case of low current discharges. For high current discharges only data from the quiescence period is presently available to provide an ensemble average power spectrum (fig. 11). (For comparison with the spectrum of thermal noise see fig. 12, which agrees well with the theoretical value).

It must be pointed out that the power spectrum of a SBD signal is different from the spectrum of the point emission, the difference being due to the integration along a chord. It can be easily demonstrated that each mode in the integration along a chord is weighted proportionally to its spatial correlation length, so that modes which are better correlated in space are favoured with respect to local fluctuations whose effect diminishes after the chord averaging. The shape of these spectra is consistent with the presence of some coherent modes at low frequency superimposed on turbulent processes whose correlation length decreases with frequency.

A similar situation was found for the structure of Zeta discharges (ref. 27) and agrees with the "tangled-discharge model" of turbulence in a reversed pinch (28 , 29). According to this model self-reversal of the magnetic field can occur as an effect of density fluctuations along the magnetic field lines together with field lines reconnections. This model predicts a cross-field correlation length for density and temperature fluctuations much shorter than the correlation length along the lines of the magnetic field ($\Lambda_\perp \sim$ 5 cm. against $\Lambda_{||} \sim$60 cm.). Similar results have been obtained both on Zeta and in more recent experiments and are confirmed by our data.

If the high frequency part of the spectrum can be interpreted roughly as due to localized random fluctuations, the low frequency part (up to 10 -20 kHz) is probably to be related to global MHD modes. In the spectrum analysis of the off-axis displacement of the centroid it was found that the frequency of the main mode (first harmonic) coincides with the peak at about 10 kHz in our spectra.

In order to investigate further details of these characteristics,

in the next section a correlation analysis is carried out in different frequency bands. Some of the results we present agree with what was already said about Zeta discharges but the scarcity of the available data does not allow any conclusive interpretation.

3.3 Correlation analysis

We move gradually from spectrum to correlation analysis and we begin the latter by calculating the cross-, phase- and coherence-spectrum for two diodes. All of them are related to the cross-correlation function which we consider later. The principles and applications of these functions are described in ref. 22 , 26 but we have to recall very briefly the major concepts: hereafter ${}^{k}x(t)$ and ${}^{k}y(t)$ will indicate the time history of the output from two diodes (the index k is for a particular realization) and ${}^{k}X(f)$ and ${}^{k}Y(f)$ their Fourier transforms.

The cross-correlation function is defined as follows:

$$R_{xy}(\tau) = < {}^{k}x(t)\,{}^{k}y(t+\tau) >$$

(the brackets indicate ensemble average).

Given the function $\Gamma_{xy}(f) = < {}^{k}X(f)\,{}^{k}Y(f)^{*} >$ the cross- and phase-spectrum are defined as the module and phase of this complex function. The coherence-spectrum is defined as follows:

$$|\gamma_{xy}(f)| = \frac{|\Gamma_{xy}(f)|}{\left\{ P_x(f)\, P_y(f) \right\}^{\frac{1}{2}}}$$

$P_x(f)$ and $P_y(f)$ being the power spectra of x(t) and y(t). The cross-spectrum (and the coherence-spectrum, its normalized version) can be thought of as a cross-correlation function in the frequency domain for the two functions X and Y calculated at zero frequency difference. Wiener-Kintchine theorem (22) relates the cross-spectrum with the cross-correlation function:

$$R_{xy}(\tau) = \int_{-\infty}^{\infty} \Gamma_{xy}(f) e^{i2\pi f\tau} \, df$$

which, for $\tau = 0$ becomes:

$$R_{xy}(o) = \langle {}^{k}x(t)\, {}^{k}y(t) \rangle = \int_{-\infty}^{\infty} \Gamma_{xy}(f) df.$$

In conclusion, one can see that cross- and coherence-spectrum are rapid means to estimate the zero-time delay correlation of two processes, each frequency of the spectrum considered separately.

Some examples of cross-, phase- and coherence-spectra are shown in fig. 13,14, for a pair of neighbouring diodes (SBD 6-SBD 7) for the case of the set-up phase of low current discharges. The peak at 10 kHz that was observed in the power spectrum is still well visible and confirms our expectation of a coherent MHD mode. At higher frequencies random fluctuations become dominant: the phase mixing produced by the line of sight integration is reflected by considerable jitter in both the phase and the coherence spectrum. Indeed high values of coherence imply low statistical variance of the spectral estimates which in turn implies small jitter on the computer-generated plots.

These preliminary results encourage us to perform a more extensive correlation analysis. Digital filtering of signals is necessary to

remove the D.C. level and to isolate each frequency band. In fact only two main frequency bands have been investigated: a "low" band from 5 to 20 kHz and a "high" band from 50 to 100 kHz. The normalized cross-correlation function is averaged over a time interval of about 700 μ s (sometimes 300 μ s) and is defined in the following way:

$$\overline{\rho_{xy}(\tau)} = \int_{t_o}^{t_o+T} \langle k_x(t) k_y(t+\tau) \rangle \, dt \Big/ \left\{ \int_{t_o}^{t_o+T} \langle k_x^2 \rangle \, dt \int_{t_o}^{t_o+T} \langle k_y^2 \rangle \, dt \right\}^{\frac{1}{2}}$$

Of course when x = y this is the auto-correlation function (similarly the cross-spectrum becomes the more familiar power spectrum).

Once again our results do not represent the point-to-point cross-correlation function because of the effect of line-of-sight integration (see ref. 30 , 31 for a study of this problem in the context of atmospheric fluctuations and interplanetary plasma turbulence). On the other hand, it is also clear that those regions of the plasma where space correlation along the direction of separation of the chords is best are bound to dominate the final result. In this way a good spatial resolution can be recovered under certain conditions, despite the averaging process inherent in the diagnostic (32). The situation is different in our case because most of the emission comes from the central hotter and denser region near the axis where the correlation across the direction of the chords is much worse than in the proximity of the reversal region (where $\vec{B}$ is aligned with the direction of separation of the lines of sight).

Spatial correlation can be displayed by plotting the cross-correlation function at zero time delay between a reference diode and all the others. The results are shown in fig. 15,16,17 for low and high current discharges, for different periods during the discharge

(setting-up phase and quiescence period) and for the two frequency bands. From these plots one can derive an estimated correlation length: for low frequency modes $\Lambda_\ell \sim 8$ -10 cm. while $\Lambda_h \sim 1$ -2 cm. in the high frequency band. (A similar plot done for the dark-current signal - when the discharge is over - shows a series of points at about 0.01-0.02: this very low but non-zero correlation is probably due to cross-talk inside the electronics and provides a good check on the reliability of this technique!).

It must be pointed out that the signal-to-noise ratio, in the quiescence period of the low current discharges, accounting for shot noise, is almost one in the "high" band and about 8-10 for the 5 to 20 kHz band (see fig. 10). This low ratio could explain the sharp step in the correlation function when approaching the origin (see fig. 16). In fact, it is easy to show how the presence of random noise modifies the zero-time delay cross-correlation of the output from two diodes:

$$\overline{\rho(0)}_{meas} = \overline{\rho(0)}_{true} \; *(1 - C), \qquad C \tilde{=} \frac{\int_{f_1}^{f_2} P_\varepsilon (f)\, df}{\int_{f_1}^{f_2} P_x (f)\, df}$$

P_ε and P_x being the power spectrum of (shot) noise and of the output voltage, respectively. The same step, however, cannot be ascribed to noise in the high current discharges (signal-to-noise ratio of order 10^2). This means that in some circumstances phenomena with different correlation lengths can occur simultaneously.

In the "low" band the correlation is never negative: this seems to indicate that MHD modes with even helicity are dominant. On the contrary the correlation function becomes negative in the "high" band

during the setting-up phase. This feature may be connected with the propagation of some kind of wave with frequency in this range. If this is so, the time-delayed cross-correlation function between diodes at increasing relative distance should show a peak gradually shifting in either direction or both (incoming and outgoing wave).

A three-dimensional plot of the cross-correlation function as a function both of time delay and of inter-diode distance would reveal such features as the propagation of a wave or the broadening of the main peak due to diffusive processes. The result of this operation is shown in fig. 18 and 19 for the "high" band in the set-up phase and during quiescence.

It appears that in the setting-up phase (fig. 18) one can detect the presence of ripples propagating in one direction. Following an earlier discussion we might wonder whether this wave propagates in the region near the axis or whether it is the "shade" of well correlated waves propagating along the magnetic field lines in the relatively cooler region near the edge (the drift waves described in ref. 33). All we can say at the moment is that in the first hypothesis the velocity of this wave would be approximately 6000 m/s and the direction point radially towards the major axis of the torus. These waves have not been observed during the quiescence phase (fig. 19).

A second array at 90 degrees in the poloidal direction from the first (using the horizontal port-hole) should not be able to detect this wave. If, on the other hand, the wave is localized to the edge of the plasma, the second array would see it propagating vertically, with the same characteristics.

4 CONCLUSION

The potential power of soft X-ray imaging as a diagnostic of RFP plasmas is amply demonstrated and in small measure realised by the results we have reported. Statistical analyses of spectral and correlation characteristics must play a more important role than in similar tokamak diagnostics, although some coherent perturbations are also observed which may be amenable to tomographic types of reconstruction.

The addition of further arrays, with the possibility of different poloidal and/or toroidal positions, is planned and should allow us to distinguish for example rotational and translational motions and also to observe the plasma further from the centre. Simply by rotating the array we can observe a section in the toroidal direction rather than the poloidal. By this means we should be able to distinguish longitudinal and transverse correlations.

The prospects are, then, that this diagnostic will provide important information about the nature of the fluctuations of the RFP and hence about the mechanisms determining the plasma parameters.

5 ACKNOWLEDGEMENTS

We are greatly indebted to Dr. P.G.Carolan who was responsible for the design of the apparatus. We also would like to thank the rest of the HBTX IA team for their help and kind support.

REFERENCES

1. S.Von Goeler: on the proceedings of the 1978 Varenna Conference on Plasma Physics Diagnostics p. 79.

2. R.Petrasso & al.:Bull. Am. Phys. Soc. 24 (1979) p.998.

3. Equipe TFR: Nucl.Fus. 17 (1977) p.1283.

4. P.Smeulders: Garching Laboratory report IPP 2-233 (1979).

5. G.L.Jahns & al.: Nucl. Fus. 18 (1978) p.609.

6. S.Von Goeler,N.R.Sauthoff,W.Stodiek: Nucl. Fus. 18 (1978) p.1445.

7. T.F.Stratton: Plasma diagnostic techniques (R.Huddlestone, S.Leonard ed.), Academic Press, New York (1965).

8. G.Cillie: Mon. Not. Roy. Astr. Soc. 92 (1932) 820.

9. G.Bertolini,A.Coche (editors): Semiconductor detectors (North Holland, Amsterdam 1968).

10. B.L.Henke & al.: in Advances in X-ray analysis (vol.13) (Plenum Press, New York 1970).

11. B.L.Henke,E.S.Ebisu: in Advances in X-ray analysis (vol.17) (Plenum Press, New York 1973).

12. W.J.Veigele: Atomic Data Tables 5 (1973) p.51.

13. J.H.Hubbel: Atomic Data 3 (1971) p.241.

14. W.R.Hunter & al.: Appl. Opt. 4 (1965) p 891.

15. R.Haensel & al.: Phys. Lett. 25A (1967) p.205.

16. R.Haensel & al.: Appl. Opt. 7 (1968) p.301.

17. N.J.Hansen: Nucl. Instr. & Meth. 96 (1971) p.373.

18. R.Petrasso & al.: Rev. Sci. Instr. 51 (1980) p.585.

19. E.Maullin: Spontaneus Fluctuations of Voltage (Oxford University Press, 1938).

20. D.Ratcliffe & al.: Culham Laboratory internal report.

21. Programs for digital signal processing: edited by the IEEE ASSP society (1979).

22. J.S.Bendat: Principles and applications of random noise theory (Chapman & Hall, London 1958).

23. D.E.Smith & al.: IEEE Transact.of Plasma Sci. PS-2 (1974).

24. S.M.Kay,S.L.Marple: Proc. IEEE, 69 (1981) p.1390.

25. K.G.Beauchamp: Signal processing using analog and digital techniques (Allen & Unwin, London 1973).

26. M.B.Priestley: Spectral analysis and time series (2 vol) (Academic Press, London 1981).

27. M.G.Rusbridge,D.C.Robinson: Phys of Fl. 14 (1971) p.2499.

28. M.G.Rusbridge: Plasma Phys. 19 (1977) p.499.

29. M.G.Rusbridge: Plasma Phys. 22 (1980) p.331.

30. S.Chandrasekhar: M.N. of Royal Astr. Soc. 112 (1952) p.475.

31. E.E.Salpeter: Astr. J. 147 (1967) p.433.

32. A.R.Jacobson: Los Alamos Sci. Laboratory report LA-8828-MS (1981).

33. A.R.Jacobson: Appl. Phys. Lett. 39 (1981) p. 795.

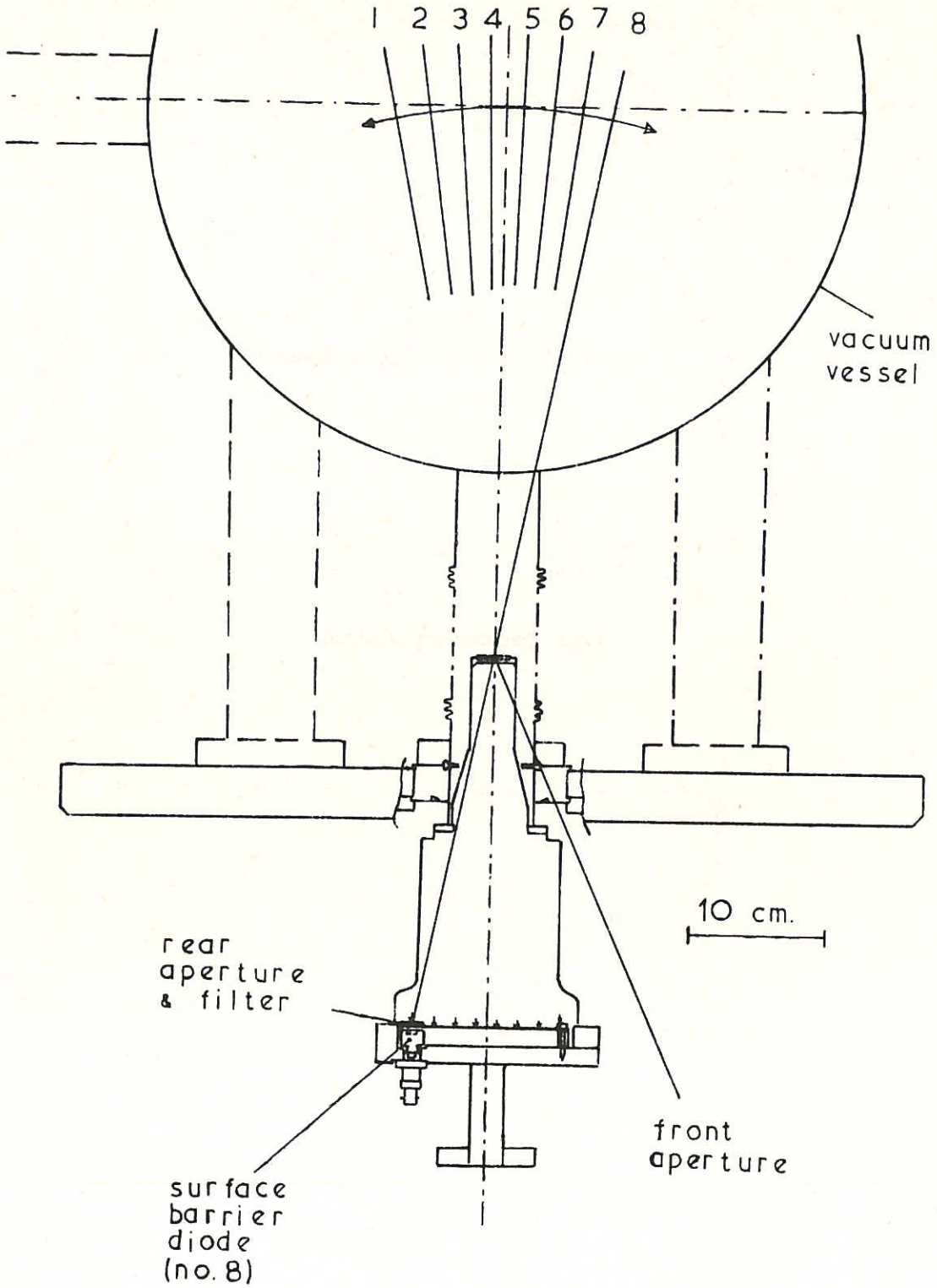

Fig.1 Geometry of the apparatus.

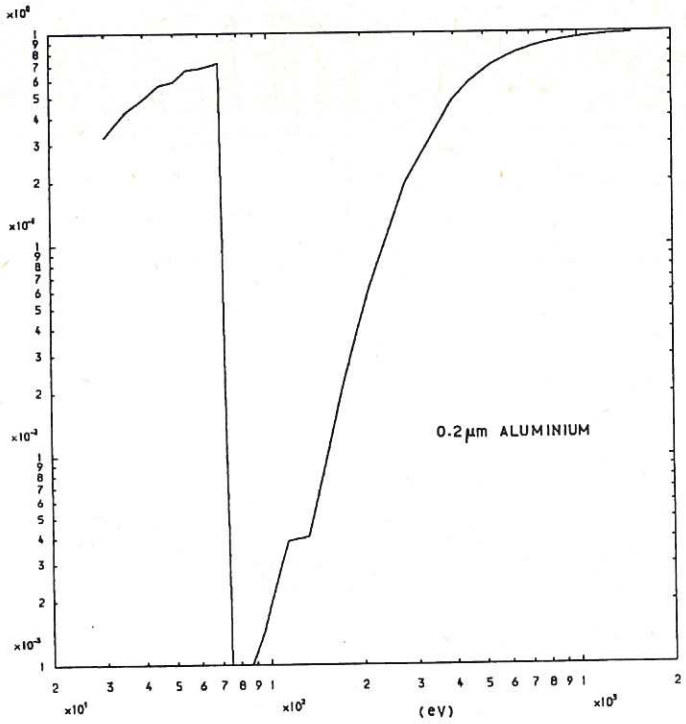

Fig.2 Transmissivity of Al foil.

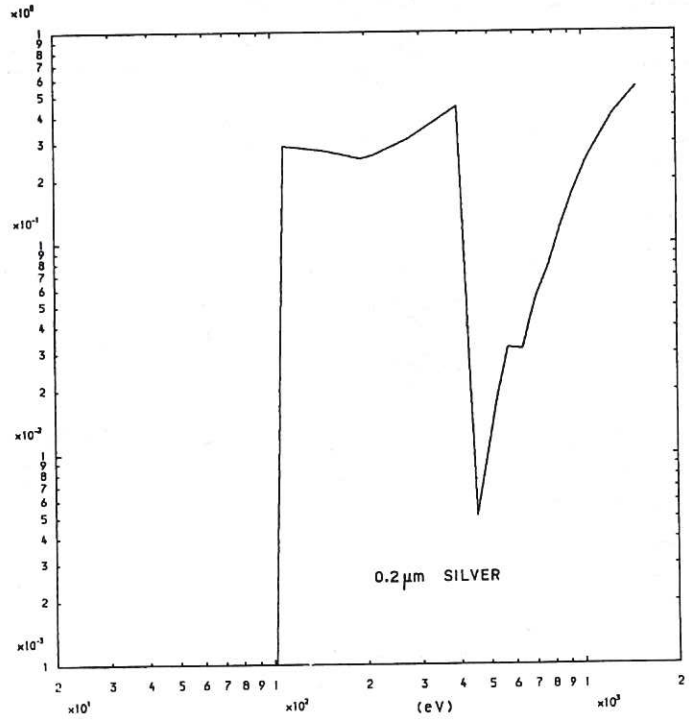

Fig.3 Transmissivity of Ag foil.

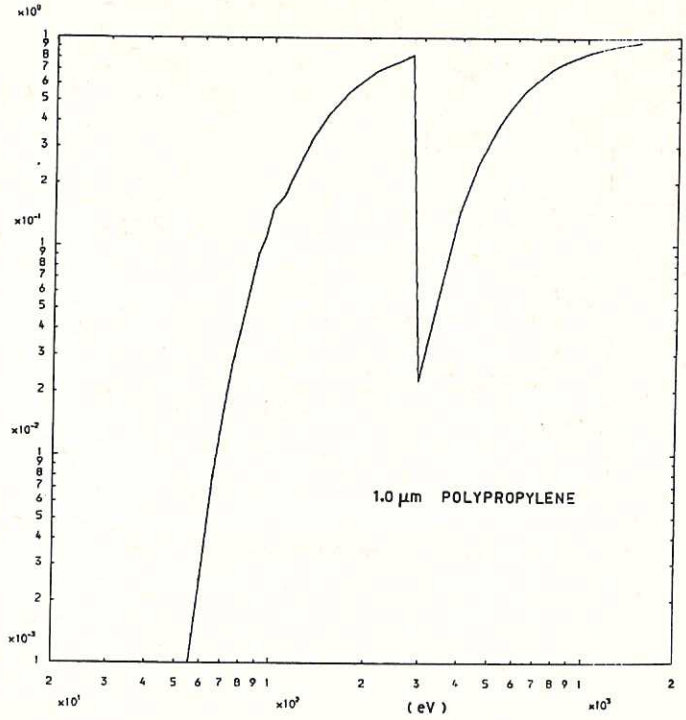

Fig.4 Transmissivity of polypropylene film.

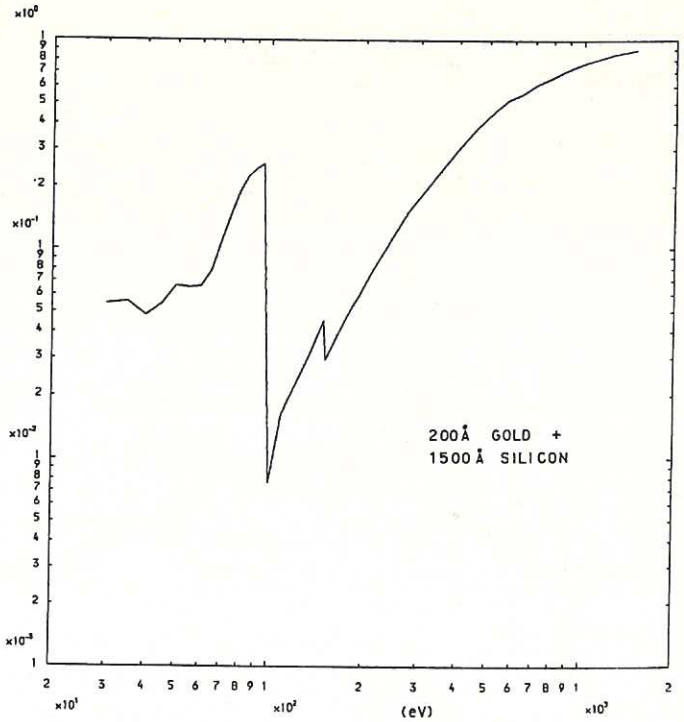

Fig.5 Detector efficiency.

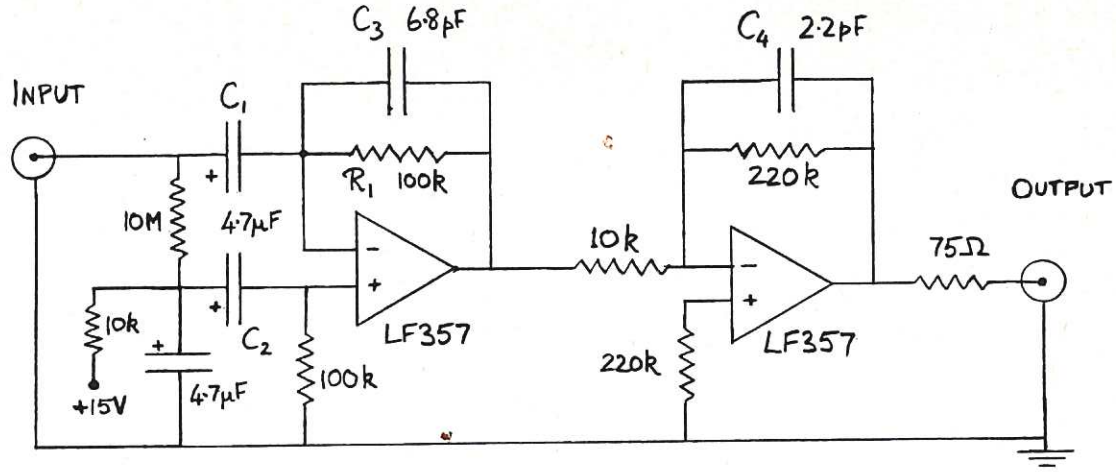

Fig.6 Preamplifier circuit.

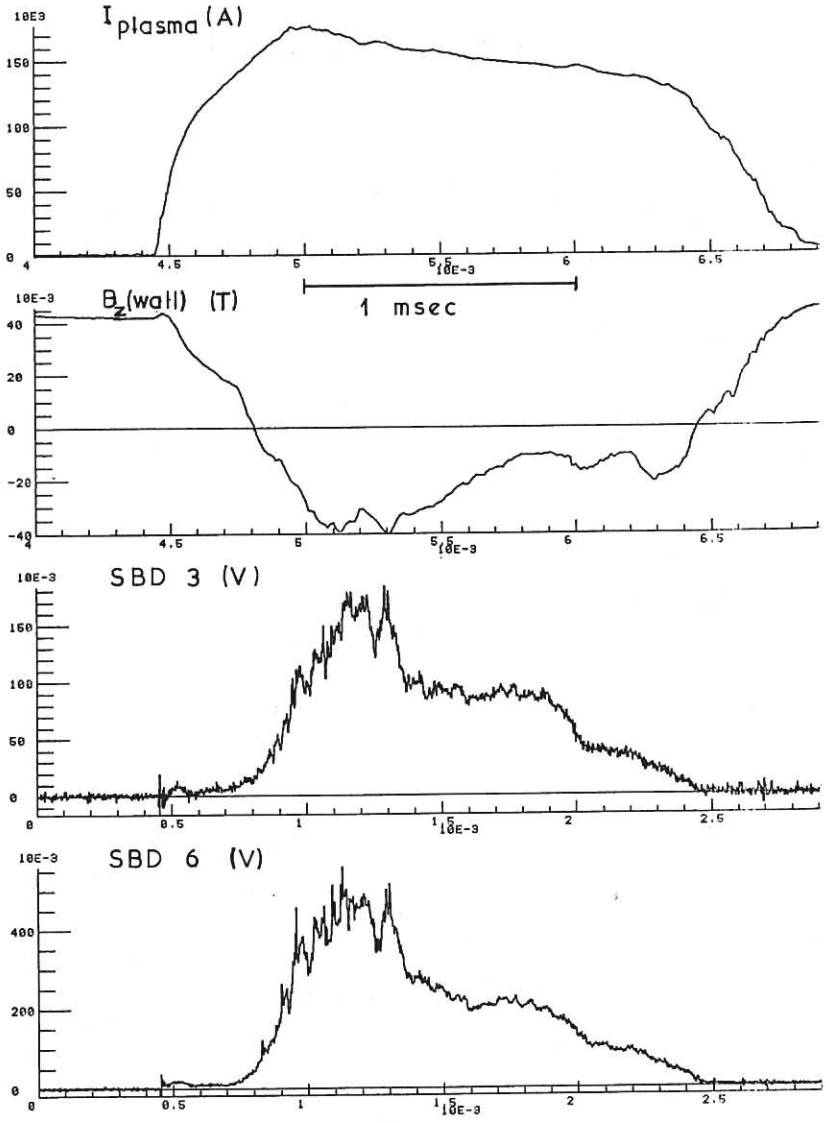

Fig.7 Typical signals of low current discharges.

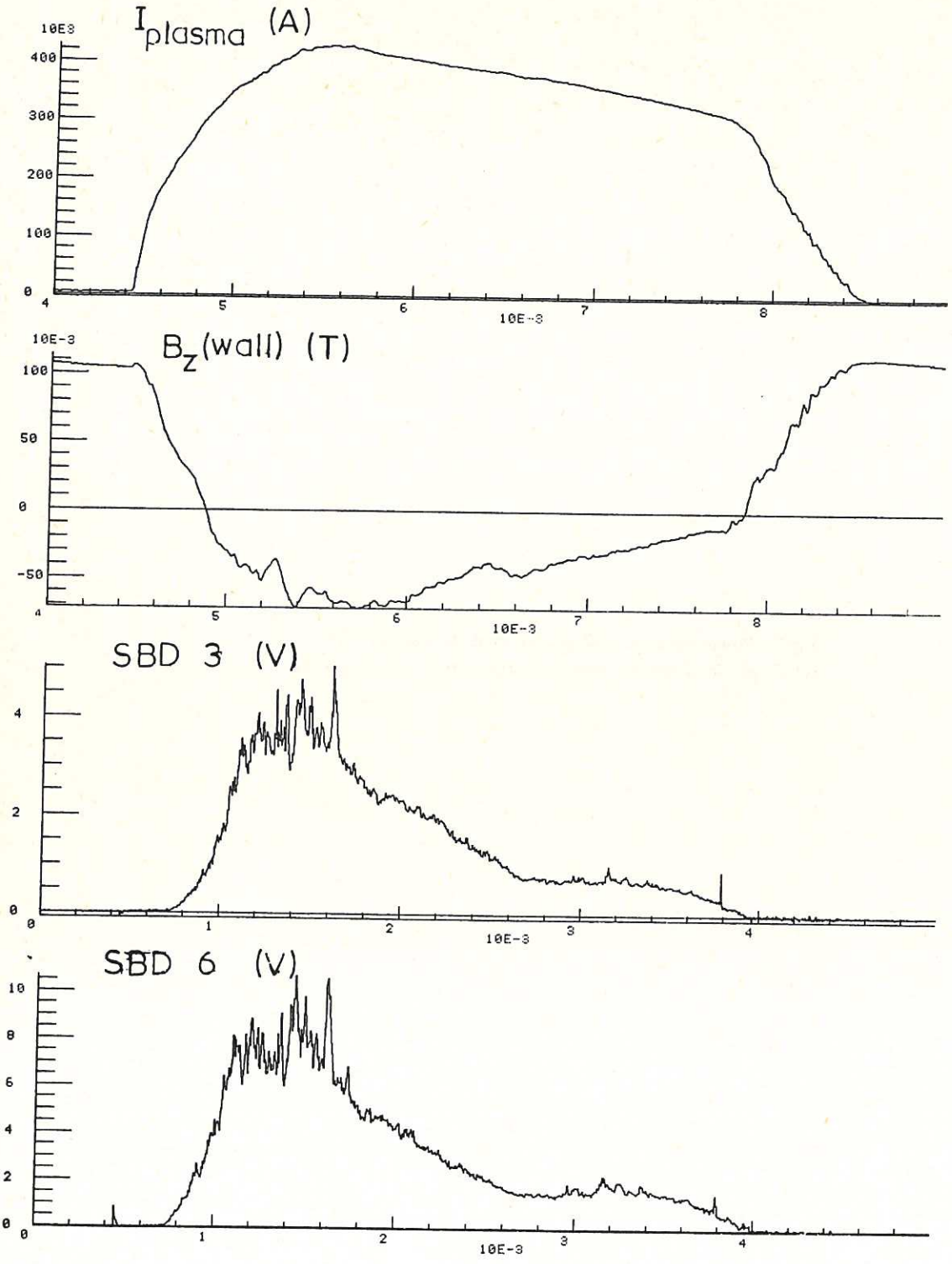

Fig.8 Typical signals of high current discharges.

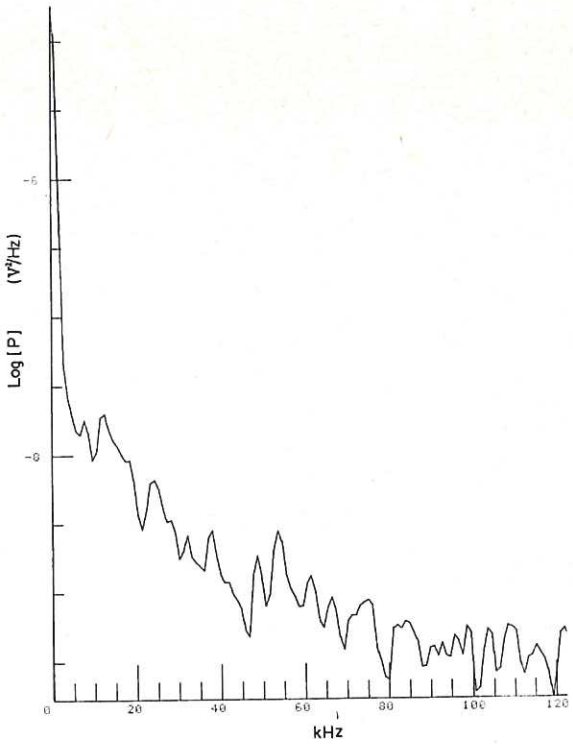

Fig.9 Power spectrum of diode output (ensemble average) in the set-up phase of low current discharges (from t_o = 0.8 ms to $t_i = t_o + 700\,\mu s$).

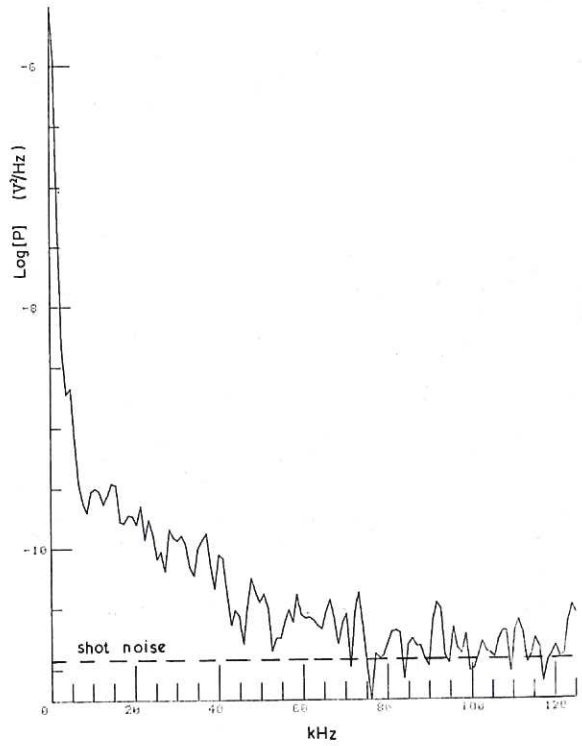

Fig.10 Power spectrum of diode output (ensemble average) in the quiescence period of low current discharges (from t_o = 1.5 ms to $t_i = t_o + 700\,\mu s$) (level of shot noise shown for comparison).

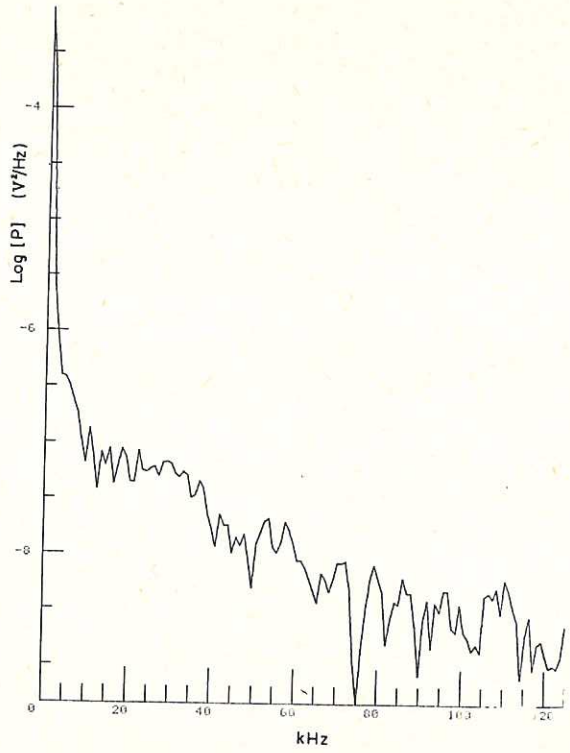

Fig.11 Power spectrum of diode output (ensemble average) in the quiescence period of high current discharges (from t_o = 2.5ms to $t_i = t_o + 700\mu s$).

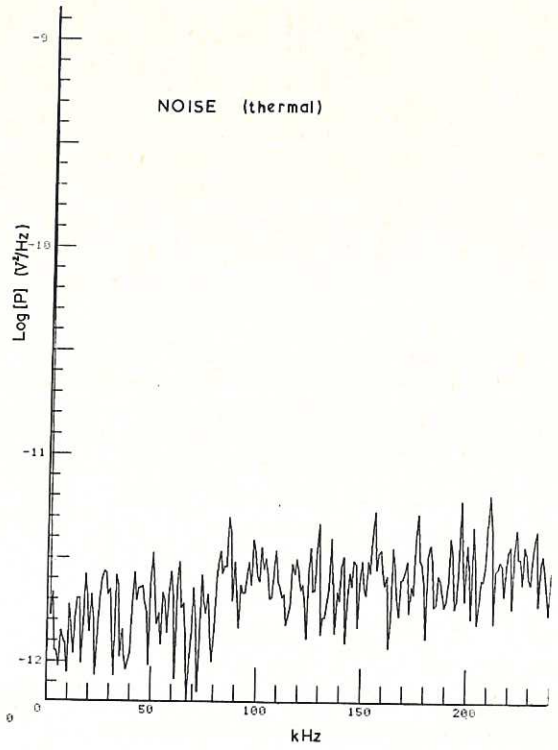

Fig.12 Power spectrum of thermal noise measured after termination of discharge.

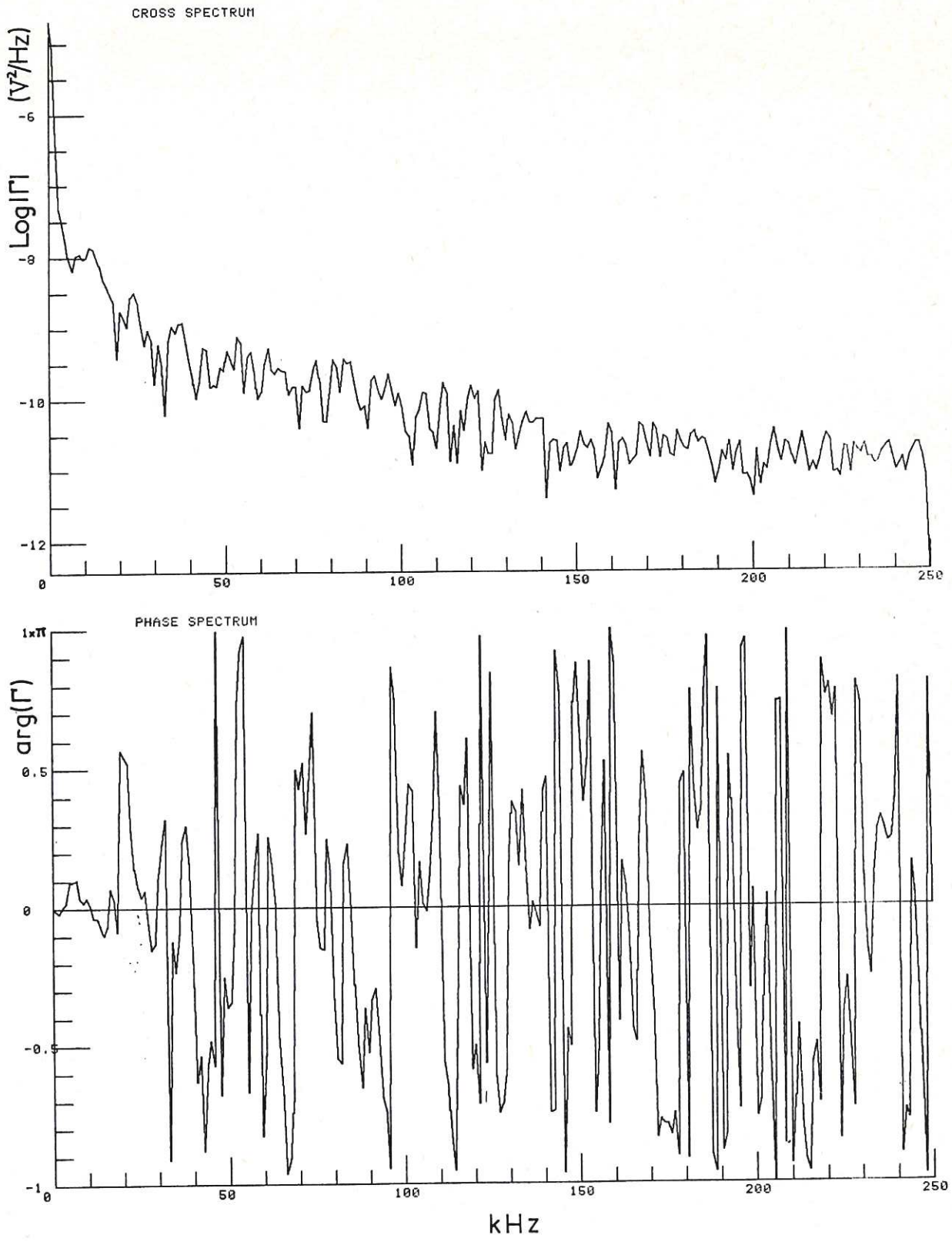

Fig.13 Cross and phase spectrum for two neighbouring diodes (set-up phase, low current discharges).

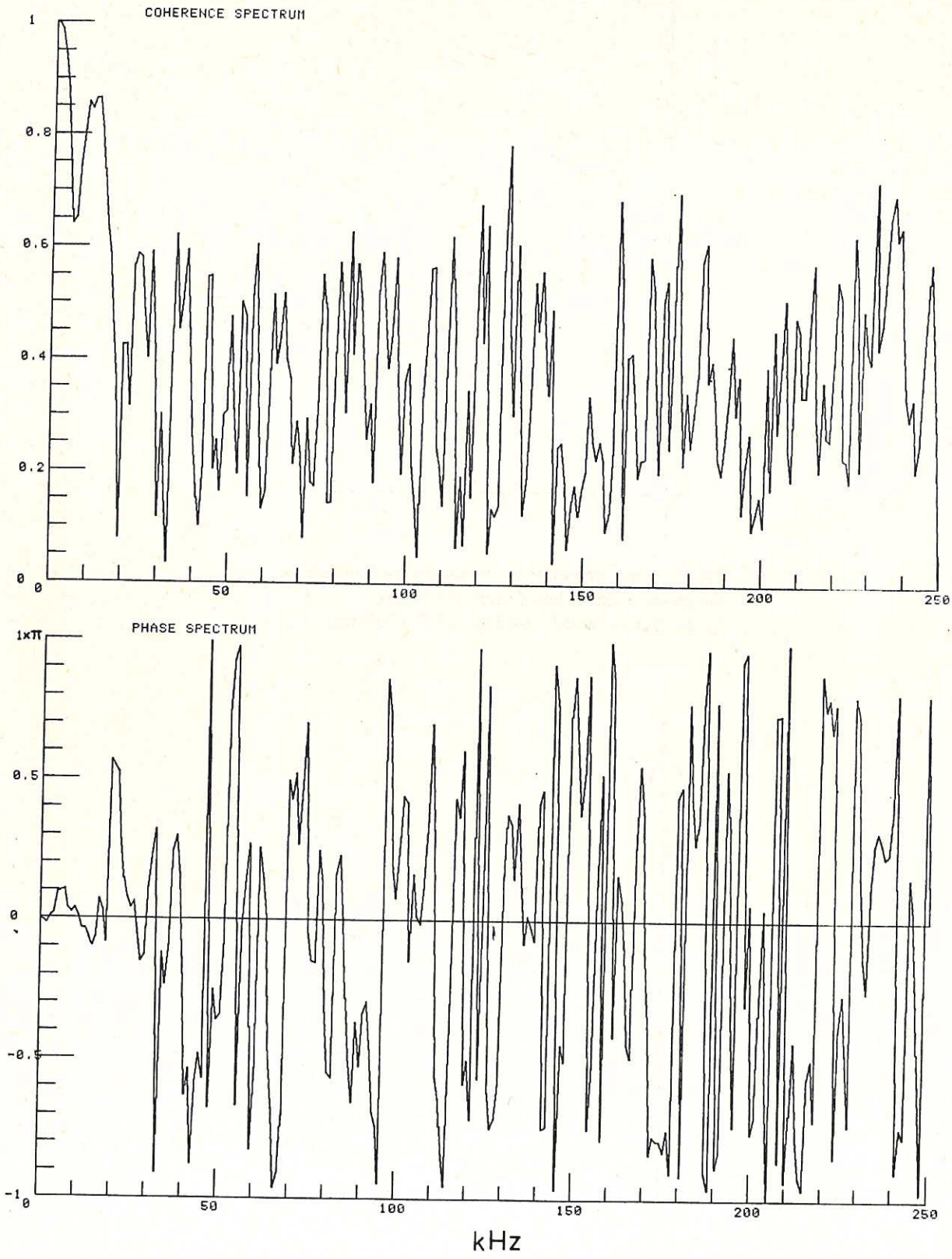

Fig.14 Coherence spectrum corresponding to the previous figure.

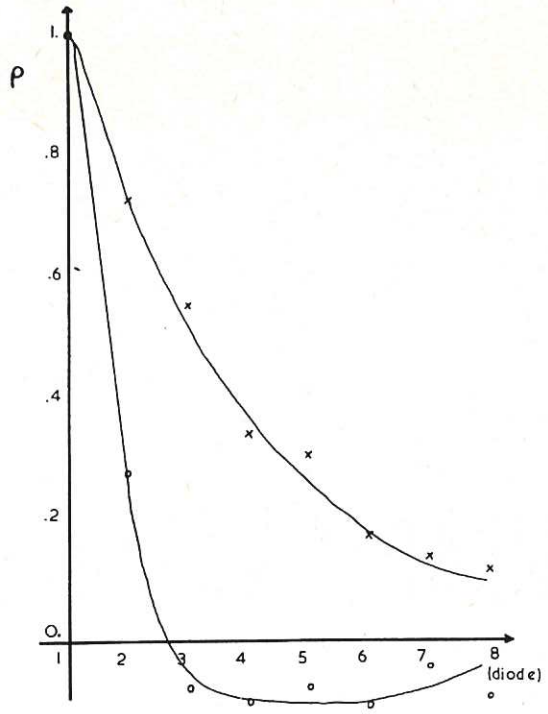

Fig.15 Zero time-delay cross-correlation function for the set-up phase of low current discharges (x: frequency band 5–20kHz, o: 50–100kHz).

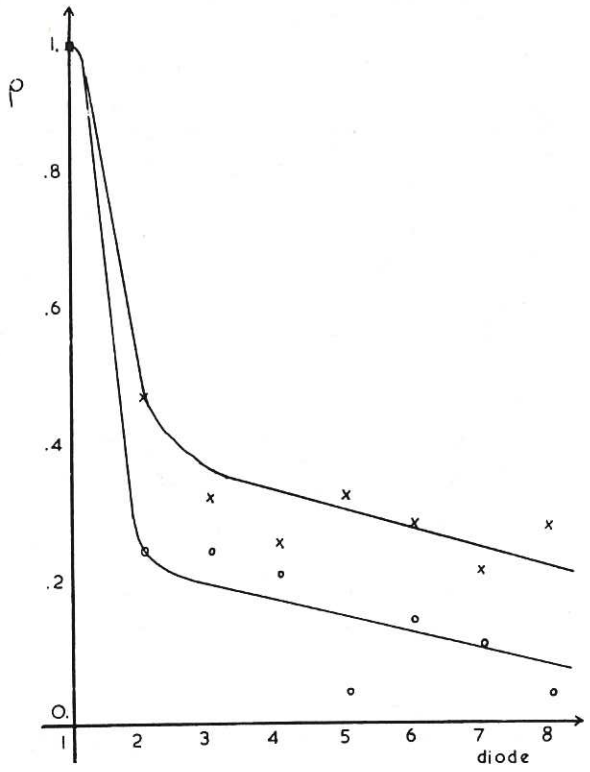

Fig.16 As before for the quiescence period of low current discharges.

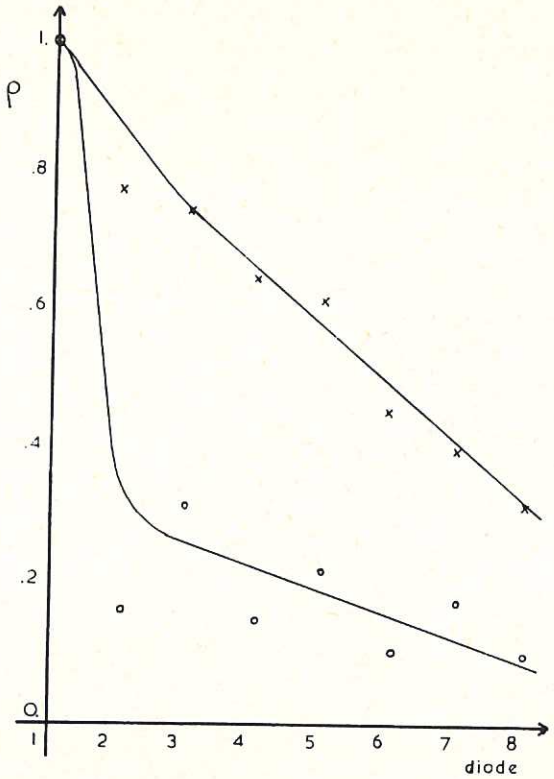

Fig.17 As before for the quiescence period of high current discharges.

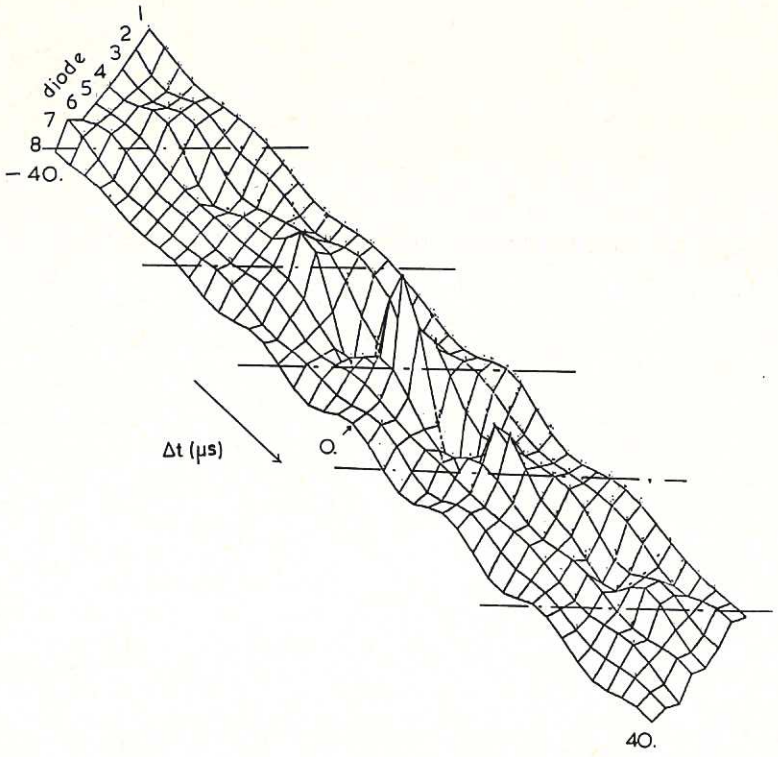

Fig.18 Time-delay cross-correlation function (set-up phase, low current discharges): some evidence of wave propagation.

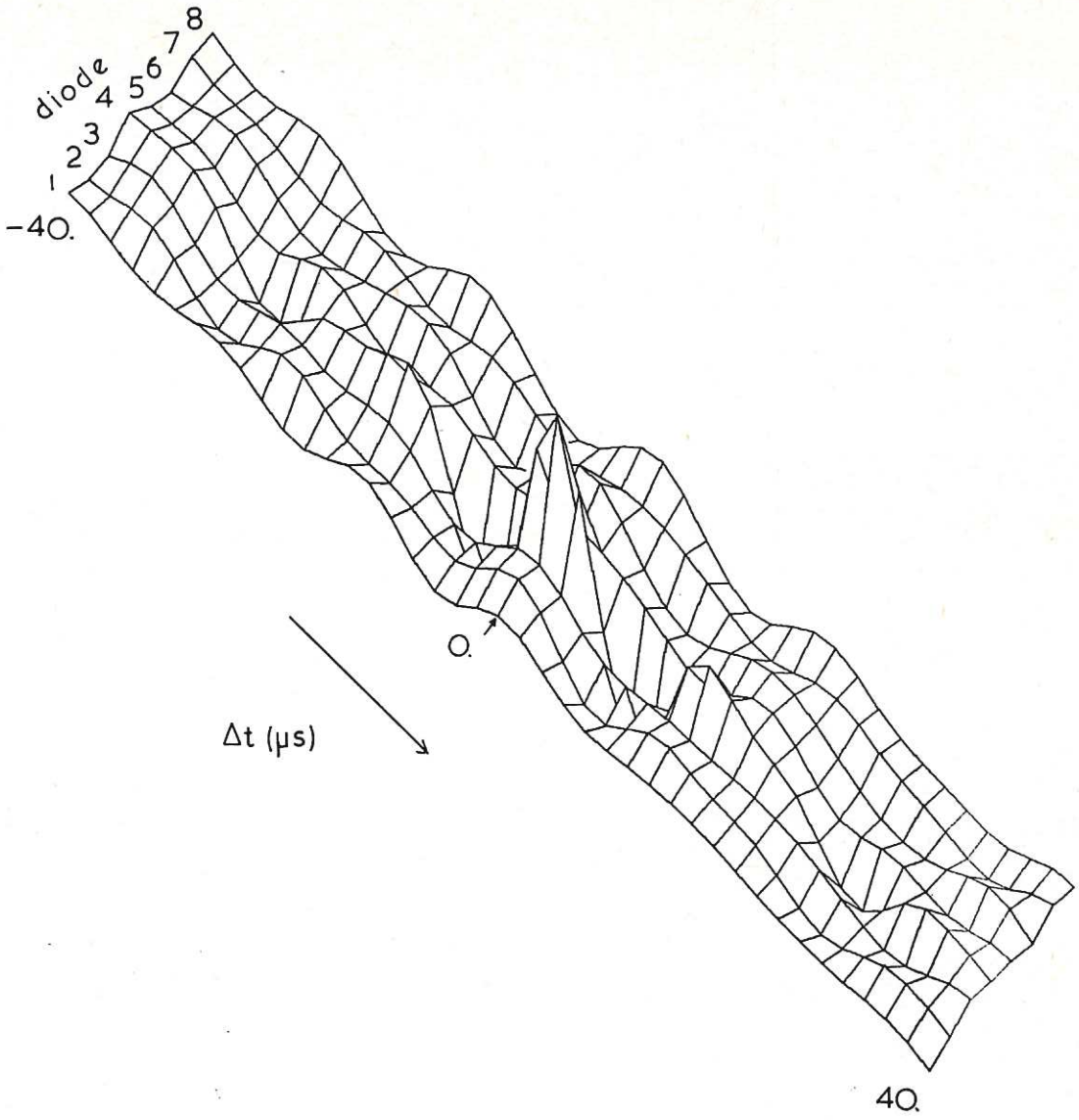

Fig.19 As before for the quiescence period (no wave propagation).

HER MAJESTY'S STATIONERY OFFICE

Government Bookshops

49 High Holborn, London WC1V 6HB
(London post orders: PO Box 569, London SC1 9NH)
13a Castle Street, Edinburgh EH2 3AR
41 The Hayes, Cardiff CF1 1JW
Brazennose Street, Manchester M60 8AS
Southey House, Wine Street, Bristol BS1 2BQ
258 Broad Street, Birmingham B1 2HE
80 Chichester Street, Belfast BT1 4JY

Publications may also be ordered through any bookseller